Orientation-Insensitive Multi-Antenna Reader for Wireless Biomedical Applications

Nilan Udayanga, Yubin Lin, and Manuel Monge
University of Southern California, Los Angeles, CA, 90089, USA
udayanga@usc.edu, yubinlin@usc.edu, and manuel.monge@usc.edu

***Abstract*—This paper presents a multi-antenna external reader system that enables orientation insensitive communication with implantable medical devices (IMDs) for wireless biomedical applications. The proposed system consists of a circular array with six loop antennas. The antenna placement and orientations are determined by analyzing the near-field magnetic field variations of the loop antenna. The proposed system is first simulated using HFSS electromagnetic simulation software. Our simulations show that the received power at the proposed external reader with six antennas only varies about 5 dB for any given orientation of the implanted antenna, which is highly significant compared to the 20-35 dB variation with a single external antenna. Here, we select the antenna which provides the largest coupling between the IMD to receive/transmit signals. A prototype of the proposed multi-antenna external reader is then implemented using custom-designed PCBs that interconnect loop antennas, transceiver ICs, and commercially-available circuit components. A custom PCB with a miniaturized loop antenna is used to emulate an implantable device. Based on measurement results, the received power in the external reader only varies about 3 dB when the miniaturized antenna rotates with respect to the x-axis. These measurements show good agreement with the simulated reader.**

***Index Terms*—Implantable medical devices, Orientation-insensitive communication, Multi-antenna external reader**

I. Introduction

Implantable medical devices (IMDs) are an integral part of the modern health care system and are used to monitor, diagnose, and treat diseases. With the advancement in IMD-based biomedical research, the number of small animal studies (e.g., mice and rats) has rapidly increased in the last two decades [1], [2]. During these studies, miniaturized IMDs are used to monitor activities in moving animals, stimulate different body parts, or deliver drugs to different parts of the body. Each of these tasks requires communication between the IMD and the external system. Conventional IMDs utilize tethered cables for communication. These cables limit the movements of the animals, affect their natural behavior, and impose a risk of infection [3]. Fully wireless IMDs address the above mentioned concerns caused by cables [4]. Wireless communication allow the animals to freely move inside the cage during the experiment without affecting their natural behavior. However, as the size of IMDs reduces, the communication with these implants becomes more challenging since the smaller size of the devices limits the area/volume of the IMD's transducer. Existing wireless technologies to communicate with IMDs are mainly based on radio frequency (RF), ultrasound, and light [2]. Contrary to ultrasound, RF signals can interact with an implant without physical contact. In addition, RF signals can reach deeper organs than light sources, as they are mostly limited to the tissue surface. However, RF methods suffer from the miniaturized antenna sizes in IMD leading to a limited communication range. More importantly, the communication range highly depend on the relative orientation between the internal antenna and the external reader, with coupling variations in the order of 20-35 dB (see Section III). This variation is highly significant for power-critical applications such as IMDs.

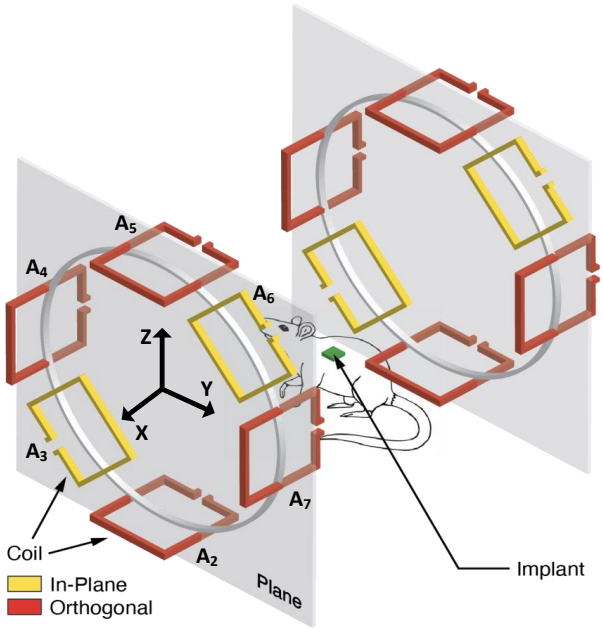

Fig. 1: Overview of the proposed multi-antenna external reader for orientation insensitive communication in a biomedical research setup.

In this article, we develop a multi-antenna external reader to establish orientation insensitive communication with IMDs. To this end, we analyzed the near-field electromagnetic field variation of the loop antenna. Fig. 1 shows the overview of the proposed external reader that enables orientation insensitive communication in a biomedical research setup.

II. Frequency and Antenna Selection

In RF techniques, IMD-to-external (uplink) or external-to-IMD (downlink) communication links are realized using either inductive coupling [5], backscattering methods [6], or near-field RF systems [7]. Inductive coupling is a short-range communication technique achieved via mutual inductance between

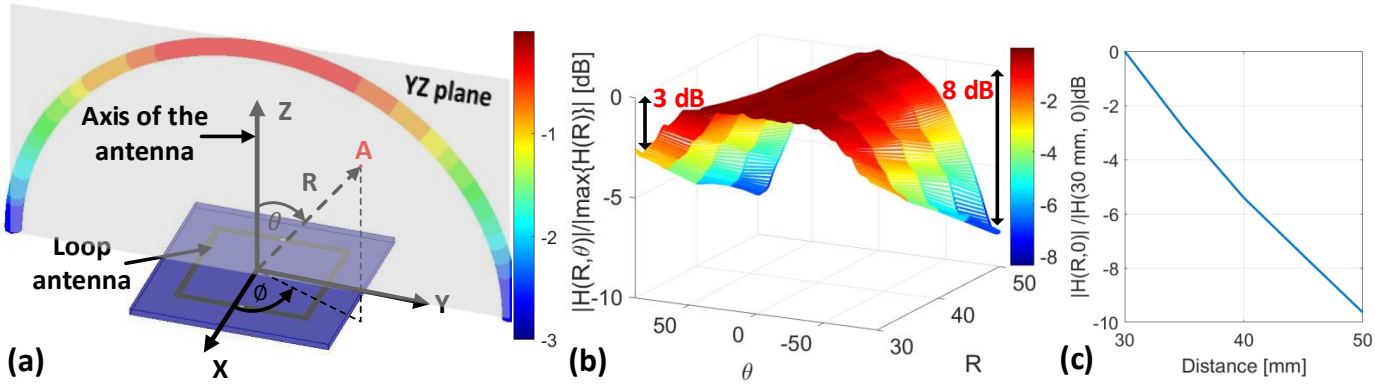

Fig. 2: (a) Spherical coordinate system to analyze the near-field of the loop antenna, which is placed on the XY plane. The normalized magnetic-field variation on the YZ plane is shown at R = 30 mm. (b) The variation of the normalized magnetic-field $|\mathbf{H}(\mathrm{R},\theta)|/|\max\{\mathbf{H}(\mathrm{R})\}|$ with the azimuth angle θ and distance R. (c) The magnetic field variation with the distance R on the z-axis. Here, the magnetic field is normalized to $|\mathbf{H}(30\mathrm{mm},0)|$.

primary and secondary coils. Both low-frequency (125-134 kHz) and high-frequency (13.56 MHz) inductive links are common in IMDs since low frequencies have better penetration in the tissues. However, they result in larger antenna sizes and low data rates. Backscattering methods remove the power-hungry active transmitters in IMDs to significantly reduce the power consumption while limiting communication range. Ultra-high frequency (402-405 MHz, 433 MHz, and 860-960 MHz) bands allow using miniaturized antennas to establish near-field and far-field RF communication links for IMDs with higher data rates. In this article, we consider a near-field RF communication link at 915 MHz to analyze and design the proposed multi-antenna external reader.

The selection of a suitable antenna type plays a critical role when designing an efficient communication link for IMDs. In general, electrical antennas such as dipoles generate a larger component of electric fields normal to the tissue interface, which results in a larger specific-absorption-rate (SAR) [8]. In contrast, the magnetic antenna's (e.g., loop antenna) electric field is tangential to the tissue interface leading to lower SAR. Furthermore, the increased permittivity inside the human body (compared to the air) significantly decreases the strong electric field at the near-field of the dipole antenna. However, the strong magnetic field of the loop antenna's near field does not degrade much since the permeability of the body does not vary significantly compared to the air. Considering all factors, loop antennas were used to design the proposed external receiver.

III. Near-field of a Loop Antenna

The proposed external reader consists of a circular array with six loop antennas that are placed on specific locations and orientations. To investigate the best orientations and the placements for each external antenna, consider a loop antenna placed at the origin on the XY plane as shown in Fig. 2(a). The magnetic field intensity at the near-field of a small loop antenna is significantly stronger compared to the electric field intensity [9]. The corresponding near-field magnetic intensity $\mathbf{H}(\mathrm{R},\theta)$ at position A is expressed as [9]

$$\mathbf{H}(\mathrm{R},\theta) = \frac{m}{4\pi \mathrm{R}^3}\left[\hat{\mathrm{R}}2\cos\theta + \hat{\theta}\sin\theta\right], \qquad (1)$$

where m is the magnetic moment of the loop and $\hat{\mathrm{R}}$ and $\hat{\theta}$ are the unit vectors in R and θ dimensions, respectively. Here, R, θ, and ϕ are the distance from the origin, elevation angle, and azimuth angle, respectively. Note that the near-field magnetic intensity on the axis of the loop ($\theta = 0$) is greater than that on the plane of the loop ($\theta = 90°$) by a factor of two (see Fig. 2 (a)). Electromagnetic simulations were performed in HFSS to examine the magnetic field variations near the rectangular loop antenna, which is used in our application. Fig. 2(b) shows the variation of the normalized magnetic field $|\mathbf{H}(\mathrm{R},\theta)|/|\max\{\mathbf{H}(\mathrm{R})\}|$ computed for different values of R and θ. This graph does not show the intensity degradation with the distance since the magnetic field is normalized to the maximum intensity at a particular distance R. The magnetic field intensity at $\theta = 0°$ is about 3-8 dB higher compared to the intensity at $\theta = \pm 90°$, for distances ranging from 30 mm to 50 mm. The above observation is valid for the near-field of both external and implantable antennas. Fig. 2(c) shows the variation of the magnetic field with the distance R, when $\theta = 0$. Here, the magnetic field is normalized to $|\mathbf{H}(30\mathrm{mm},0)|$.

IV. Proposed Multi-Antenna External Reader

Now consider a single external antenna with a miniaturized implanted antenna as shown in Fig. 3(a). The coupling coefficient (or the scattering parameter $|\mathbf{S}_{21}|$) between the implanted antenna A_1 and the external antenna A_2 is calculated using HFSS simulations by placing the two antennas 50 mm apart (center to center). The implanted antenna is placed 10 mm away from the air-tissue interface. Here, we consider muscle tissues with proper permittivity and conductivity values. The tissue is modeled as a cylinder with 10 mm radius. Consider the two external antenna orientations shown in Fig. 3(a). In orientation **I**, the axis of the external antenna is directed towards the implant, whereas in orientation **II**, the implanted antenna is on the plane of the external antenna. Fig. 3(b) shows the variation of the normalized coupling coefficient ($|\mathbf{S}_{21}|_n$) when the plane of the implanted antenna rotates with respect to the x-axis, where ψ is the rotation angle ($0° \leq \psi \leq 180°$). Initially, the plane of the implanted antenna is on the XY plane ($\psi = 0°$).

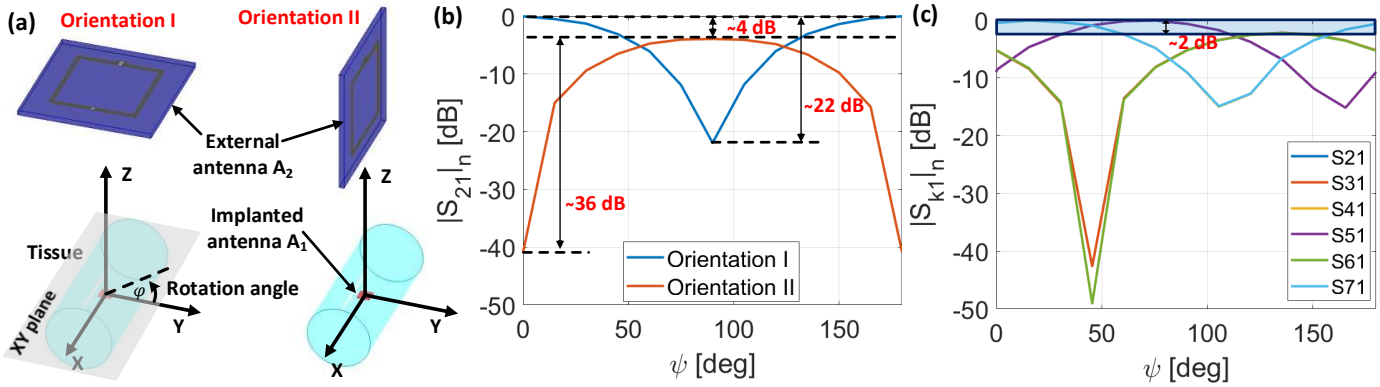

Fig. 3: (a) Different external antenna orientations. Variation of the coupling coefficients when the implanted antenna rotates with respect to the x-axis: (b) with a single external antenna (orientations **I** and **II**), (c) with the multi-antenna external reader.

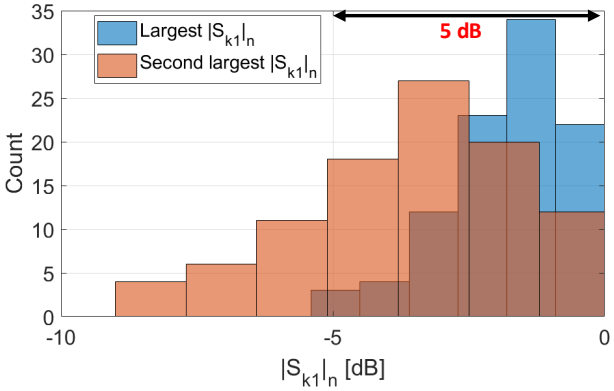

Fig. 4: Histograms of the largest and the second-largest coupling coefficient values when the orientation of the implanted antenna is varied randomly with respect to x-, y-, and z-axes (simultaneously).

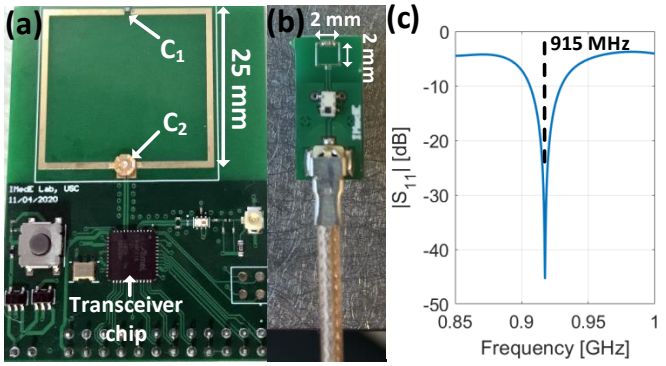

Fig. 5: (a) External transceiver PCB with the loop antenna and the transceiver IC. (b) PCB with the miniaturized loop antenna. (c) Measured reflection coefficient ($|S_{11}|$) of the antenna.

The two antenna orientations show different coupling profiles due to different polarizations of the external antennas. As an example, in orientation **I**, both antennas are in the same polarization at $\psi = 0°$ and $\psi = 180°$, leading to a peak coupling at these angles, whereas their polarizations are orthogonal to each other at $\psi = 90°$, leading to the minimum coupling coefficient. In contrast, orientation **II** provides the peak coupling at $\psi = 90°$. These simulation results provide two key insights. First, the coupling between the two antennas can vary about 20-35 dB with the orientation of the implanted antenna, if the external system only consists of a single antenna. Thus, the implanted transceiver needs to significantly increase the transmit power for certain orientations during the uplink communication. For the downlink, even though the external antenna can easily increase the transmit power, the maximum SAR levels need to be maintained, which limits the downlink communication range for certain orientations. Second, even though both orientations provide a similar 3 dB angle ($\sim$90°), orientation **I** provides about 4 dB higher coupling coefficient when the two antennas are in the same polarization (due to the factor 2 in (1)). This implies that when placing multiple external antennas, it is better to have a larger number of antennas with their axes directed towards the implanted antenna.

Based on the above results, a circular array with six antennas (A_2 to A_7) is proposed to establish an orientation insensitive communication link between the implanted antenna and the external reader (see Fig. 1). There are two antennas parallel to each major planes (XY, YZ, and XZ). Note that the axes of four out of six antennas are directed towards the implant. Planes of A_2-A_5 and A_4-A_7 antenna pairs are parallel to XY and XZ planes, respectively. Planes of A_3 and A_6 antennas are on the YZ plane. Each antenna pair provides significant coupling when the orientation of the implanted antenna is closer to the particular plane (closer to the same polarization). Redundancy is used here (two antennas instead of one antenna per plane) to enable position insensitive communication for IMDs, which we will explore in future work. As an example, one of the A_2 and A_5 antennas can provide a significant coupling when the implant moves along the z-axis. Thus, the three antenna pairs not only cover the orientations of the implanted antenna but also the movements along the axes to a greater extent. Fig. 3(c) shows the variation of the normalized coupling coefficients when the implanted antenna is rotated with respect to the x-axis. We select the antenna with the largest coupling for communication. Thus, the coupling between the implanted antenna and the external reader only varies about 2 dB for every orientations. As a future work, we will explore near-field beamforming techniques to further reduce the variation.

Similarly, we can observe the variation of the coupling coefficient when the implanted antenna rotates with respect to all axes. Here, we performed a Monte Carlo simulation

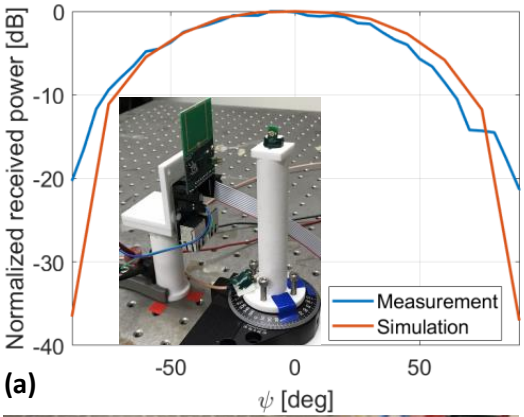

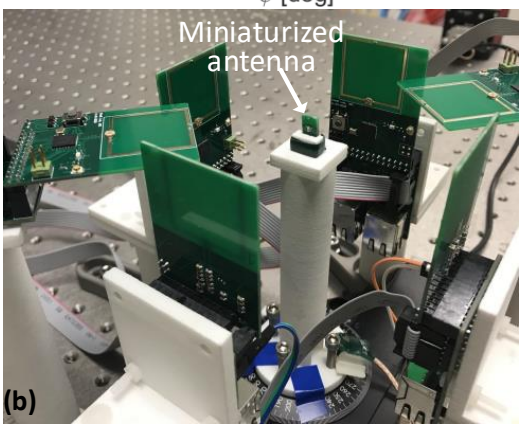

Fig. 6: (a) Comparison between the simulated and measured received power (normalized) variation with the orientation of the miniaturized antenna. A single external antenna is considered (measurement setup is also shown here). (b) Prototype multi-antenna reader.

by randomly varying the implanted antenna orientation with respect to x-, y-, and z-axes, simultaneously. Fig. 4 shows the histograms of the largest and the second-largest $|\mathbf{S}_{k1}|_n$ values for 100 different random orientations. A uniform distribution is considered for the random variation. If we select the antenna with the largest $|\mathbf{S}_{k1}|_n$, the coupling only varies about 5 dB for any given orientation of the implanted antenna, which is highly significant compared to the 20-35 dB variation with a single external antenna.

V. Prototype Multi-antenna Reader and Measurements

A prototype of the proposed multi-antenna external reader is implemented using custom-designed PCBs that interconnect a loop antenna, Microchip's AT86RF215-ZUR RF transceiver IC, and commercially-available circuit components (see Fig. 5(a)). The loop antenna size is 25 mm×25 mm. The input impedance of the antenna is matched to the IC by utilizing the split capacitor matching technique (using capacitors C_1 and C_2). These capacitors can be used to control both impedance and the resonance frequency. A tunable capacitor is used as capacitor C_2 to compensate for PCB fabrication variations. The transceiver IC is controlled/programmed using a microcontroller. Fig. 5(b) shows the miniaturized loop antenna, which is used to emulate an IMD. The loop antenna size is selected as 2 mm x 2 mm so that it can be easily integrated

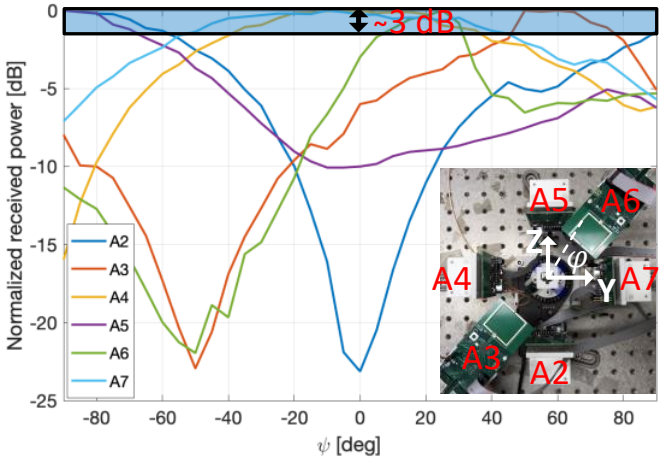

Fig. 7: The variation of the measured received power (normalized) at each external antenna with the orientation of the miniaturized antenna.

with miniaturized systems [10]. Both antennas are fabricated using FR-4 base material with controlled impedance. The self-resonance frequencies of the external and the miniaturized antennas are 1.06 GHz and about 11 GHz, respectively. Fig. 5(c) shows the measured reflection coefficient ($|S_{11}|$) of the loop antenna, which resonates at 915 MHz.

The received power is measured in dB at a single external antenna by varying the orientation of the miniaturized antenna as shown in Fig. 6(a). The miniaturized antenna is rotated using a motorized rotation platform. Fig. 6(a) also shows the variation of the measured received power (normalized) when the orientation of the miniaturized antenna varies from -90° to +90°. The figure also compares the measurements with the simulation results, which shows a good fit with the simulated antenna. Fig. 6(b) shows the complete measurement setup of the proposed multi-antenna reader. The received power at each antenna is measured in dB by varying the orientation of the miniaturized antenna with respect to x-axis. The antenna is at the origin of the circular array. Fig. 7 shows the corresponding normalized power results. Based on the measurements, the received power only varies about 3 dB for any given orientation of the miniaturized antenna, which shows an agreement with the simulated reader.

VI. Conclusion

In this paper, we demonstrate an orientation insensitive communication platform for wireless biomedical applications. The proposed external reader consists of a circular array with six loop antennas. The orientations and the placements of each antenna of the array were determined by analyzing the near-field magnetic fields of the loop antenna. Based on the electromagnetic simulations, the received power at the external reader only varies about 5 dB for any given orientation of the implanted antenna, which is highly significant compared to the 20-35 dB variation with a single external antenna. A prototype of the proposed system is implemented using custom-designed PCBs and commercially available circuit components. Measurement results show a good agreement

with the simulated multi-antenna reader. In our future work, we will explore the proposed external reader towards enabling position and orientation insensitive communication for IMDs.

ACKNOWLEDGEMENTS

The authors would like to thank the funding support of USC and NIH/NIBIB under award number R21EB030244.

REFERENCES

[1] B. Ellenbroek and J. Youn, "Rodent models in neuroscience research: is it a rat race?" *Disease models & mechanisms*, vol. 9, no. 10, pp. 1079–1087, 2016.

[2] L. Luan *et al.*, "Recent advances in electrical neural interface engineering: Minimal invasiveness, longevity, and scalability," *Neuron*, vol. 108, no. 2, pp. 302–321, 2020.

[3] S. M. Won and et al., "Wireless and battery-free technologies for neuroengineering," *Nature Biomedical Engineering*, pp. 1–19, 2021.

[4] B. Lee *et al.*, "An implantable peripheral nerve recording and stimulation system for experiments on freely moving animal subjects," *Scientific reports*, vol. 8, no. 1, pp. 1–12, 2018.

[5] Y. Shi *et al.*, "A 10 mm3 inductive coupling radio for syringe-implantable smart sensor nodes," *IEEE Journal of Solid-State Circuits*, vol. 51, no. 11, pp. 2570–2583, 2016.

[6] A. Khaleghi, A. Hasanvand, and I. Balasingham, "Radio frequency backscatter communication for high data rate deep implants," *IEEE Transactions on Microwave Theory and Techniques*, vol. 67, no. 3, pp. 1093–1106, 2019.

[7] B. Zhao and et al., "A batteryless padless crystalless 116 μ m $\times$ 116 μ m "dielet" near-field radio with on-chip coil antenna," *IEEE Journal of Solid-State Circuits*, vol. 55, no. 2, pp. 249–260, 2020.

[8] K. S. Nikita and et al., *Wireless Mobile Communication and Healthcare*. Springer, 2011.

[9] C. A. Balanis, *Antenna theory: analysis and design*. John Wiley & Sons, 2016.

[10] M. L. Wang and et al., "Wireless data links for next-generation networked micro-implantables," in *2018 IEEE Custom Integrated Circuits Conference (CICC)*, 2018, pp. 1–9.